This article has been accepted for publication in a future issue of this journal, but has not been fully edited. Content may change prior to final publication. Citation information: DOI 10.1109/TIE.2020.3008377, IEEE Transactions on Industrial Electronics

Efficient Control-Oriented Coupled Electrochemical Thermal Modeling of Li-Ion Cells

Matteo Corno

***Abstract*—Safe and effective exploitation of Lithium Ion batteries requires advanced battery management systems (BMS). This paper proposes a computationally efficient, control-oriented model of a Li-ion cell. The model describes the spatial nature of both the chemical species and temperature dynamics in a computationally efficient way. The method takes advantage of the algebraic structure that arises from the distributed nature of the model. We show that, by discretizing the model partial differential equations with a finite difference method, the coupling equations take a semi separable structure for which an efficient algebra exists. This approach yields an efficient modeling tool that can be employed to design model-based estimation and control algorithms. The proposed model is validated against a high order computational fluid dynamics (CFD) model showing accuracy and efficiency.**

I. Introduction

Due to their chemical properties, Li-ion batteries require battery management systems (BMS's). BMS's continuously monitor and control the battery states: temperature, current, voltage, amount of remaining energy, and battery degradation. Many of these variables are not directly measurable.

There exist mainly two families of BMS's: rule-based and model-based. Rule-based BMS's avoid critical conditions for the battery by setting limits on measurable variables. Model-based BMS's exploit the knowledge of the internal dynamics of the cell to estimate non measurable variables and control their dynamics [1]. Model-based control and estimation outperforms rule-based BMS's and the more accurate the model is, to the fuller the battery potential can be exploited.

Several models of Li-ion batteries exist. They are classified according to their complexity (see for example [2]). The simplest models a BMS can employ are static voltage and current limits. The introduction of dynamics yields better performance. The simplest dynamical models are the equivalent circuit models (ECM's) [3]. ECM's are sufficiently accurate for relatively low and constant currents; however they fail to describe the cell dynamics for medium-high dynamic currents; furthermore they offer no physical insight into the electrochemical phenomena taking place inside the cell.

First-principle electrochemical models, or *white-box* models overcome these limitations [4]. The pseudo 2-dimensional (P2D) electrochemical model, originally proposed in [5], [6] and adopted in works such as [7]–[9], is widely recognized as a valuable trade-off between detailed modeling and computational cost. It assumes spherical active material particles and it considers only two dimensions: the radial dimension, r, and the cell film thickness, named x. The P2D model, relying on partial differential algebraic equations (PDAEs), requires particular care in the implementation. Several methods are available in literature to find approximated and/or reduced-order solutions [10]–[12].

The original formulation of the P2D model does not account for thermal dynamics; however, a number of thermal models have been developed for Li-ion cells [13]. A family of approaches use lumped thermal models, see for example [14]–[18], where the temperature gradient is neglected or modeled with two states [19]. This hypothesis breaks under high discharge rate [20]. Other models are not bidirectionally coupled, in the sense that they account for the effect of the electrochemical processes on the heat generation, but neglect the converse effect [21]. This drawback is overcome in [22] where the classical P2D model of a cylindrical cell is coupled with a lumped thermal model, making the physiochemical properties of the cell temperature dependent. The most complete approaches consider the coupled electrochemical thermal model [23], [24]. These methods are often not suited for real-time applications and do not provide a model that is mathematically manipulable for BMS design.

In this article, which extends the work presented in [25], we present a new formulation of the P2D model for a cylindrical cell. We focus on the following main contributions:

- We augment the standard P2D model with thermal dynamics. The proposed coupling is bi-directional and spatially distributed. The thermal model considers that the heat generation mechanisms depend on the local value of the electrochemical states. This overcomes the limitation of the lumped approaches [14]–[18] as the higher resolution of the distributed thermal model can better capture the thermal dynamics especially during high current events.
- We propose an efficient integration scheme. We recast the nonlinear equations of the P2D model in a distributed framework. This, with minor approximations, determines the rise of specific algebraic structure, the semi separable structure (SSS) [26]. For such systems, it is possible to use an efficient structure-preserving arithmetic. Matrix

Matteo Corno is with the Dipartimento di Elettronica, Informazione e Bioingegneria, Politecnico di Milano, 20133 Milano, Italy. Email addess matteo.corno@polimi.it. This work was supported by MIUR SIR project RBSI14STHV

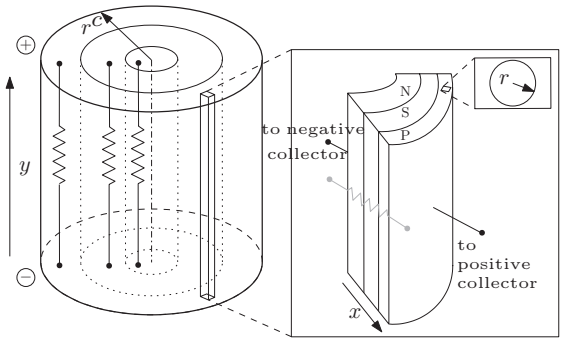

Fig. 1. Layout of a cylindrical Li-ion cell.

Fig. 2. Sectional photograph of a cylindrical Li-Ion cell showing the sandwich structure.

addition, multiplication, inversion and norm are computed with $O(N)$ or in some cases $O(1)$ complexity; for comparison, with classical arithmetics the same operations would be carried out with $O(N^3)$ complexity. The method represents a third way with respect to the ones employed in the literature that are often based on model reduction [27] or other approximation techniques for partial differential equations [28].

- In addition to the computational efficiency, the SSS approach has two additional advantages applicable to the design of control and estimation algorithms: it yields a closed form cell model that can be used to design estimation and control algorithm as the variables retain their original physical meaning and there exist efficient techniques for the design of control and estimation algorithms for SSS systems (see for example [29], [30]).

The paper is structured as follows. Section II recalls the partial differential equations that determine both the electrochemical and thermal dynamics. Section III presents the discretization approach and the coupling between the thermal and electrochemical parts. Section IV introduces the computationally efficient framework based on the semi separable structure. Section V analyzes the model from the dynamic and computational effort stand points.

II. Lithium Ion Cell Modeling

We refer to the standard P2D model which considers only the diffusion dynamics that take place across the battery film thickness, x, and the diffusion dynamics inside the spherical particles, along the *radial direction* r (see Fig. 1, 2 and 3). The

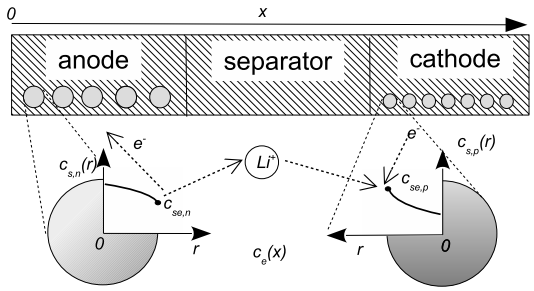

Fig. 3. Schematic representation of the P2D model and the dual intercalation process.

dynamics of interest can be divided into the electrochemical dynamics and the thermal dynamics.

A. Electrochemical Dynamics

This section recalls the fundamental characteristics of the well-known P2D model. The reader is referred to [31] for a more complete discussion and nomenclature. In what follows, t represents the time, x the spatial coordinate along the x-direction and r the spatial coordinate along the radius of the active material sphere. $c_e(t,x)$ represents the Li^+ concentration in the electrolyte, $c_s(t,r,x)$ the concentration of Li in the solid phase; $\phi_s(x,t)$ and $\phi_e(x,t)$ are respectively the potential in the solid and electrolyte phases. i_s is the electronic current in solid phase; i_e is the ionic current in electrolyte phase; ϕ_s is the potential of solid phase; ϕ_e is the potential of electrolyte phase. D_s is the solid phase diffusion coefficient; F is the Faraday's constant; a_s is the specific interfacial area of an electrode; D_e^{eff} is the electrolyte phase effective diffusion coefficient; t_+^0 is the transference number of Li^+ (assumed constant); σ^{eff} is the effective conductivity; k^{eff} is the effective ionic conductivity, while k_D^{eff} is the effective diffusion conductivity coefficient. A few geometrical quantities are defined as well: A is the electrode plate area; δ_n, δ_s and δ_p are, respectively, the thickness of the negative and positive electrodes and separator; $L = \delta_n + \delta_s + \delta_p$ is the overall film thickness. T is the absolute temperature. Fig. 5 summarizes the equations that describe the electrochemical dynamics:

Mass balances. These PDE's describe the conservation of Li in the solid and electrolyte phases. The reaction current j^{Li} determines the coupling between the two phases.

Charge balances. These PDE's, through modified Ohm's laws, describe the charge migration.

Kinetics. The above PDE's are coupled by the Butler-Volmer equation describing the reaction current at the solid/electrolyte interface:

$$j^{Li}(x) = a_s j_0 \left[\exp\left(\frac{\alpha_a F}{RT}\eta\right) - \exp\left(-\frac{\alpha_c F}{RT}\eta\right) \right] \quad (1)$$

where α_a and α_c stand for the anodic and cathodic transfer coefficients; R is the universal gas constant; j_0 is the exchange current density and η is

$$\eta = \phi_s - \phi_e - U(c_{s,e}). \quad (2)$$

The equilibrium (open circuit) voltage $U(c_{s,e})$ is evaluated as a non linear empirical function of the surface stoichiometry.

This article has been accepted for publication in a future issue of this journal, but has not been fully edited. Content may change prior to final publication. Citation information: DOI 10.1109/TIE.2020.3008377, IEEE Transactions on Industrial Electronics

The electrochemical dynamics depend on the temperature; in particular, j_0, the diffusion coefficient in the solid phase D_s, the diffusion coefficient in the electrolyte phase D_e and the electrolyte ionic conductivity K depend on the temperature following the Arrhenius equation:

$$\Psi(T) = \Psi_{ref} \exp\left[\frac{E^{\Psi}_{act}}{R}\left(\frac{1}{T_{ref}} - \frac{1}{T}\right)\right]$$

where Ψ is the generic parameter taken into account, Ψ_{ref} is the value of the parameter at the reference temperature T_{ref}, E^{Ψ}_{act} is the activation energy of the physiochemical property.

Terminal voltage. The cell potential is given by,

$$V = \phi_s(x = L) - \phi_s(x = 0) - \frac{R_f}{A} I \tag{3}$$

where R_f is the film resistance of the electrodes surface and I the cell current.

B. Thermal dynamics

We are considering a cylindrical cell obtained by wounding a large *sandwich* of positive electrode, separator and negative electrode. In this configuration, the current between the electrode runs radially to the cell, we thus assume that the largest temperature gradients develop along the *radial direction r* (see [32], [33]); as a consequence, we can use the 1D heat conduction in a cylinder:

$$\rho c_p \frac{\partial T}{\partial t} = k_t \frac{\partial^2 T}{\partial^2 r^c} + \frac{k_t}{r^c}\frac{\partial T}{\partial r^c} + Q \tag{4}$$

with boundary conditions:

$$\left.\frac{\partial T}{\partial r^c}\right|_{r^c=0} = 0, \qquad \left.\frac{\partial T}{\partial r^c}\right|_{r^c=R^c} = -\frac{h}{k_t}(T - T_\infty). \tag{5}$$

In the above equations, and using the SI units, T_∞ is the environment temperature, k_t is the thermal conductivity, ρ is the density, h is the convection heat transfer coefficient, c_p is the specific heat capacity, r^c and R^c are the radial direction and the radius of the cylinder. Considering a heterogeneous cylinder, the heat capacity C_p is calculated as proposed in [33]:

$$C_p = \rho c_p = \sum_{i,k} \frac{\delta_i \varepsilon_{k,i} \rho_{k,i} c_{p,k,i}}{L} \tag{6}$$

where k indicates the phase (solid or electrolyte) and i the component (negative electrode, separator, positive electrode). Furthermore, δ_i is the thickness of the i-th component and ε_k is the volume fraction of the k-th phase in the i-th component. The volumetric heat generation rate, Q, is the sum of three terms: the volumetric reaction heat Q_j, the volumetric ohmic heat Q_o, the volumetric heat generated due to contact resistance Q_f:

$$Q_j = \frac{1}{h^c}\int_0^L j^{Li}\eta\, dx, \quad Q_f = \frac{R_f}{h^c}\left(\frac{I}{A}\right)^2,$$

$$Q_o = \frac{1}{h^c}\int_0^L \sigma^{eff}\left(\frac{\partial \phi_s}{\partial x}\right)^2 + k^{eff}\left(\frac{\partial \phi_e}{\partial x}\right)^2 + \\ + k_D^{eff}\left(\frac{\partial ln(c_e)}{\partial x}\right)\left(\frac{\partial \phi_e}{\partial x}\right) dx.$$

In the above expressions, Q_j is due to the electrochemical dual-intercalation reaction taking place at the active material particles surface; Q_0 is the heat generated by the conduction of charges in materials with limited conductivity. Q_f is the heat generated by the contact resistance R_f between the electrodes and the current collectors. Finally, h^c is the height of the cylinder. Note the dependency on electrochemical variables, which determines the coupling between the two domains (thermal and electrochemical).

III. Discretization Approach

In a cylindrical cell, the electrochemical and the thermal spatial distributions develop in two different directions. The electrochemical equations have x and r as spatial dimensions whereas the thermal PDE develops over the cell radius r^c. As a consequence, we cannot employ a single discretization scheme. We will thus discuss the electrochemical equation discretization first, then the thermal equation and finally the coupling. In discretizing both domains, we opted to employ a semi-discrete approach [34]. First, we discretize only in space so to leave the problem continuous in time. In the second stage, we integrate those equations in time using standard ODE tools. The semi-discrete is versatile as it allows for more freedom in choosing the spatial and temporal discretization and integration techniques independently.

A. Electrochemical dynamics

Fig. 4 graphically describes how the model of Fig. 3 can be discretized in a finite difference approach. The method assumes that the positive and negative electrodes consist of a series of spherical active material particles, each occupying one slice of the discretization along x with step Δx. The

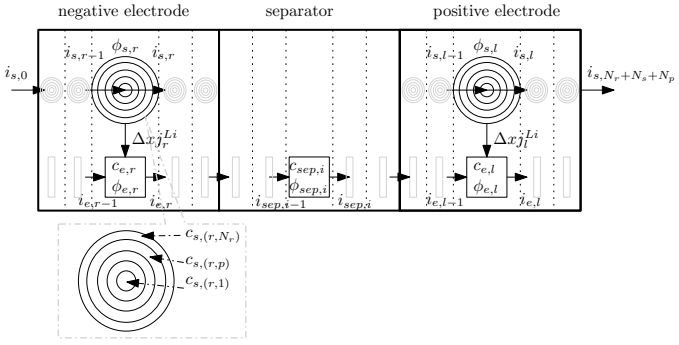

Fig. 4. Discretization of Li-ion cell along x and r dimensions.

second discretization axis is the radial dimension r of each spherical active material particle. This discretization step is Δr. N_r, N_n, N_s and N_p are respectively the number of finite elements of the sphere, of the negative electrode, of the separator and of the positive electrode discretization. Each discretized region has a lumped electrolyte phase Li^+ concentration c_e and electrolyte phase potential ϕ_e (named c_{sep} and ϕ_{sep} in the separator). Each sphere has a lumped solid phase potential ϕ_s and a volumetric rate of electrochemical reaction, j^{Li}, while the solid phase Li concentration is distributed along r. The currents, i_s and i_e, exhibit a gradient along x. Fig.

This article has been accepted for publication in a future issue of this journal, but has not been fully edited. Content may change prior to final publication. Citation information: DOI 10.1109/TIE.2020.3008377, IEEE Transactions on Industrial Electronics

Species: solid phase	
$\frac{\partial c_s}{\partial t} = \frac{D_s}{r^2}\frac{\partial}{\partial r}\left(r^2\frac{\partial c_s}{\partial r}\right)$	$\dot{c}_{s,(k,p)} = \frac{D_s}{(p\Delta r)^2}\left[2p\Delta r\left(\frac{c_{s,(k,p+1)}-c_{s,(k,p)}}{\Delta r}\right) + (p\Delta r)^2\left(\frac{c_{s,(k,p-1)}-2c_{s,(k,p)}+c_{s,(k,p+1)}}{\Delta r^2}\right)\right]$
$\left.\frac{\partial c_s}{\partial r}\right\|_{r=0} = 0$ $D_s\left.\frac{\partial c_s}{\partial r}\right\|_{r=R_s} = \frac{-j^{Li}}{a_s F}$	$c_{s,(k,1)} - c_{s,(k,0)} = 0$ $D_s\left(\frac{c_{s,(k,N_r+1)}-c_{s,(k,N_r)}}{\Delta r}\right) = \frac{-j_k^{Li}}{a_s F}$
Species: electrolyte phase	
$\frac{\partial \varepsilon_e c_e}{\partial t} = \frac{\partial}{\partial x}\left(D_e^{eff}\frac{\partial c_e}{\partial x}\right) + \frac{1-t_+^0}{F}j^{Li}$	$\dot{c}_{e,k} = \frac{D_e^{eff}}{\varepsilon_e}\left(\frac{c_{e,k-1}-2c_{e,k}+c_{e,k+1}}{\Delta x^2}\right) + \frac{1-t_+^0}{F}j_k^{Li}$
$\left.\frac{\partial c_e}{\partial x}\right\|_{x=0} = 0$ $\left.\frac{\partial c_e}{\partial x}\right\|_{x=L} = 0$	$c_{e,1} - c_{e,0} = 0$ $c_{e,N_n+N_s+N_p+1} - c_{e,N_n+N_s+N_p} = 0$
Charge: solid phase	
$i_s = -\sigma^{eff}\frac{\partial \phi_s}{\partial x}$	$i_{s,k} = -\sigma^{eff}\left(\frac{\phi_{s,k+1}-\phi_{s,k}}{\Delta x}\right)$
$\left.\frac{\partial \phi_s}{\partial x}\right\|_{x=\delta_n} = \left.\frac{\partial \phi_s}{\partial x}\right\|_{x=\delta_n+\delta_s} = 0$ $-\sigma^{eff}\left.\frac{\partial \phi_s}{\partial x}\right\|_{x=0} = -\sigma^{eff}\left.\frac{\partial \phi_s}{\partial x}\right\|_{x=L} = \frac{I}{A}$	$i_{s,N_n} = i_{s,N_n+N_s} = 0$ $i_{s,0} = i_{s,N_n+N_s+N_p} = \frac{I}{A}$
Charge: electrolyte phase	
$i_e = -k^{eff}\frac{\partial \phi_e}{\partial x} - k_D^{eff}\frac{\partial}{\partial x}ln(c_e)$	$i_{e,k} = -k^{eff}\left(\frac{\phi_{e,k+1}-\phi_{e,k}}{\Delta x}\right) - k_D^{eff}\left(\frac{ln(c_{e,k+1})-ln(c_{e,k})}{\Delta x}\right)$
$\left.\frac{\partial \phi_e}{\partial x}\right\|_{x=0} = 0$ $\left.\frac{\partial \phi_e}{\partial x}\right\|_{x=L} = 0$	$\phi_{e,1} - \phi_{e,0} = 0$ $\phi_{e,N_n+N_s+N_p+1} - \phi_{e,N_n+N_s+N_p} = 0$

Fig. 5. Electrochemical model equations and their discretization.

5 summarizes the governing equations and their discretized versions. The model has $(N_r+1)N_p + (N_r+1)N_n + N_s$ dynamic equations, coupled by j_k^{Li} through a non-linear algebraic system.

B. Thermal dynamics

The thermal dynamics are discretized with a finite difference method along the radial direction. The cell is divided in a number (N_c) of concentrical cylindrical cells with Δr^c step, determined according to a constant volume approach. The discretization of (4) results in:

$$\rho c_p \dot{T}_z = k_t\left[\frac{T_{z-1}-2T_z+T_{z+1}}{(\Delta r_z^c)^2}\right] + \frac{k_t}{r_z^c}\left[\frac{T_{z+1}-T_z}{\Delta r_z^c}\right] + Q_z$$

where the subscript z indicates the discretized cell. The term Δr_z is defined as: $\Delta r_z^c = r_z^c - r_{z-1}^c$ where: $r_0^c = 0$ and $r_{N_c}^c = R^c$ with boundary conditions

$$T_1 - T_0 = 0, \qquad \frac{T_{N_c+1}-T_{N_c}}{\Delta r_{N_c}^c} = -\frac{h}{k_t}(T_{N_c} - T_\infty).$$

C. Coupling

The two discretization approaches need to be mapped one onto the others. Cylindrical cells are obtained by winding up a thin sandwiched sheet in a cylinder (Fig. 1). The Li-ion cell is thus viewed as N_c subcells in parallel where each subcell is described by an electrochemical set of equations and characterized by its own temperature. The thermal model describes the heat diffusion through the different subcells. The coupling is determined by the Arrhenius equation. The discretized heat generation rate Q_z of the z-th subcell is:

$$Q_z = Q_{j,z} + Q_{o,z} + Q_{f,z}, \quad Q_{j,z} = \frac{1}{h^c}\sum_i j_{i,z}^{Li}\eta_{i,z}\Delta x$$

$$Q_{f,z} = \frac{R_f}{h^c A_z^2}\left(\widehat{I}_z\right)^2$$

$$Q_{o,z} = \frac{1}{h^c}\sum_i\left[\sigma^{eff}\left(\frac{\phi_{s,i+1,z}-\phi_{s,i,z}}{\Delta x}\right)^2\Delta x\right] + \frac{1}{h^c}\sum_i\left[k^{eff}\left(\frac{\phi_{e,i+1,z}-\phi_{e,i,z}}{\Delta x}\right)^2\Delta x\right] + \frac{1}{h^c}\sum_i\left[k_D^{eff}\left(\frac{ln(c_{e,i+1,z})-\ln(c_{e,i,z})}{\Delta x}\right)\left(\frac{\phi_{e,i+1,z}-\phi_{e,i,z}}{\Delta x}\right)\Delta x\right]$$

The term $\widehat{I}_z$ represents the input current of the z-th subcell. The parallel connection of the subcells impose that:

$$I = \sum_{z=1\ldots N_c}\widehat{I}_z \tag{7}$$

The model has $N_c\left[(N_r+1)(N_n+N_p)+N_s\right]$ ODE's, that are coupled by the Butler-Volmer equation in groups of $\left[(N_r+1)(N_n+N_p)+N_s\right]$ and a set of N_c-1 constraint-type-equations:

$$V_{z+1} - V_z = 0 \quad \text{with} \quad z \in [1, N_c-1]. \tag{8}$$

The coupling of the impedance-like causality of the P2D model with these constraints is not trivial. The following section introduces a numerical efficient integration scheme to treat the system.

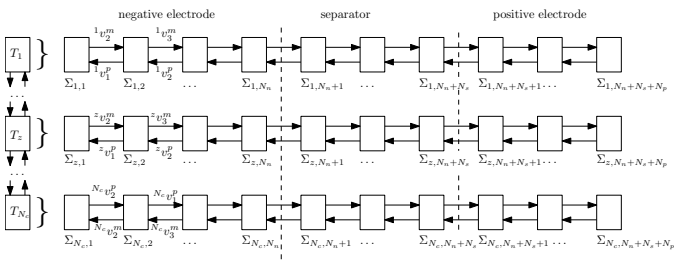

Fig. 6. Li-ion cell as spatially distributed string interconnected system.

IV. Integration Scheme

The proposed integration scheme stems from considering the discretized system as a Spatially Interconnected System. The cells represent a series of dynamical systems that communicate through interface variables. The communication happens on different scales: each element of the electrochemical

$$E = \begin{bmatrix} O_1 & P_1R_2 & P_1Q_2R_3 & P_1Q_2Q_3R_4 & \ddots & \vdots \\ L_2N_1 & O_2 & L_2R_3 & L_2Q_3R_4 & \ddots & \vdots \\ L_3M_2N_1 & B_3^mN_2 & O_3 & L_3R_4 & \ddots & \vdots \\ L_4M_3M_2N_1 & B_4^mM_3N_2 & B_4^mN_3 & O_4 & \ddots & \vdots \\ \ddots & \ddots & \ddots & \ddots & \ddots & P_{N-1}^pN_N \\ \dots & \dots & \dots & \dots & L_NN_{N-1} & O_N \end{bmatrix} \tag{12}$$

discretization communicates with the adjacent ones and each string of cell is influenced by the other strings through the thermal dynamics.

A. Spatially Interconnected Systems

Let us consider Fig. 6 and use the index $k \in [0, ..., N_{tot}]$ to indicate each subsystem in a string, and the index z to indicate the row obtaining $\Sigma_{z,k}$ as in figure. In addition, the superscript m indicates the connecting variables from system k to $k+1$, whereas the superscript p refers to the connecting variables from $k+1$ to k. According to this structure, each subsystem has its own state variables x, and dynamic equation f that uses the interconnecting variables v as inputs, and three output equations: to compute the interconnecting variables and one (if present) the measurable outputs. If, to simply the notation, we drop the row index notation, each system in a string can be written as:

$$\begin{aligned} \dot{x}_k &= f_k\left(x_k, v_k^p, v_k^m, u_k\right) \\ v_{k-1}^p &= g_k^p\left(x_k, u_k, v_k^p, v_k^m\right) \\ v_{k+1}^m &= g_k^m\left(x_k, u_k, v_k^p, v_k^m\right) \\ y_k &= h_k\left(x_k, v_k^p, v_k^m, u_k\right) \end{aligned} \tag{9}$$

and take the name of spatially distributed string interconnected system [26]. Such systems can be either strictly spatially proper or not depending on whether g_k^p and g_k^m are dependent on v_k^m and v_k^p, respectively. Let us start considering a strictly spatially proper system. In this case, the interconnecting variables can be easily eliminated through a process called *lifting*; this yields a $N_{tot}N_{sub}$ order system (N_{sub} being the order of the subsystem). The computational complexity of integrating the complete system with standard ODE solvers grows as $\mathrm{O}\big((N_{tot}N_{sub})^3\big)$.

On the other hand, preserving the distributed nature of the system and simulating each subsystem independently yields an improvement of computational efficiency. This idea is based on sampling the interconnecting variables at frequency h. The integration routine simulates the N_{tot} subsystems independently at a shorter integration step and computes the interface variables at a lower sampling rate. This approximation yields a computational complexity to $\mathrm{O}\big(N_{tot}N_{sub}^3\big)$ or even $\mathrm{O}\big(N_{sub}^3\big)$ - if a parallel architecture with N_{tot} cores is available. Note that the under sampling of the interconnecting variables may introduce errors. The entity of the errors depend on how much the internal dynamics are coupled to the dynamics of the interconnecting variables.

In the case of non spatially strictly proper systems the situation is more complex. If g_k^p or g_k^m are dependent on v_k^m and v_k^p, it is, in general, not possible to write the subsystems in explicit form. The case of linear dependency represents a special case for which we propose an efficient method. Assume that

$$\begin{aligned} \dot{x}_k &= f_k\left(x_k, v_k^p, v_k^m, u_k\right) \\ v_{k-1}^p &= g_{k1}\left(x_k, u_k\right) + W_k^p v_k^p + Z_k^m v_k^m \\ v_{k+1}^m &= g_{k2}\left(x_k, u_k\right) + Z_k^p v_k^p + W_k^m v_k^m \\ y_k &= h_k\left(x_k, v_k^p, v_k^m, u_k\right) \end{aligned} \tag{10}$$

then the interconnecting equations can be arranged in a linear system of the form $Ev = b(x, u)$ where,

$$v = \begin{bmatrix} v_1^p \\ v_2^m \\ v_2^p \\ \vdots \\ v_{N-1}^m \\ v_{N-1}^p \\ v_N^m \end{bmatrix} \quad b = \begin{bmatrix} g_{12}\left(x_1, u_1\right) \\ g_{21}\left(x_2, u_2\right) \\ g_{22}\left(x_2, u_2\right) \\ \vdots \\ g_{(N-1)1}\left(x_{(N-1)}, u_{(N-1)}\right) \\ g_{(N-1)2}\left(x_{(N-1)}, u_{(N-1)}\right) \\ g_{N1}\left(x_N, u_N\right) \end{bmatrix}. \tag{11}$$

The spatially distributed nature of the system makes E a sequentially semi separable matrix [26] encoded as in (12) (at the top of the page) where,

$$\begin{aligned} &L_s = \begin{bmatrix} I \\ 0 \end{bmatrix} \ \forall s \in \{2, 3, \cdots, N-1\}, \ L_N = I \\ &M_s = 0 \ \forall s \in \{2, 3, \cdots, N-1\} \\ &N_1 = I, \ N_s = \begin{bmatrix} 0 & I \end{bmatrix} \ \forall s \in \{2, 3, \cdots, N-1\} \\ &O_1 = -Z_1^p, \ O_N = -Z_N^m \\ &O_s = \begin{bmatrix} -Z_s^m & -W_s^p \\ -W_s^m & -Z_s^p \end{bmatrix} \ \forall s \in \{2, 3, \cdots, N-1\}, \\ &P_1 = I, \ P_s = \begin{bmatrix} 0 \\ I \end{bmatrix} \ \forall s \in \{2, 3, \cdots, N-1\} \\ &Q_s = 0 \ \forall s \in \{2, 3, \cdots, N-1\} \\ &R_s = \begin{bmatrix} I & 0 \end{bmatrix} \ \forall s \in \{2, 3, \cdots, N-1\}, \ R_N = I. \end{aligned} \tag{13}$$

Sequentially semi separable matrices (SSS) define an algebra for which efficient algorithms exist. In particular, the system of equations $Ev = b(x,u)$ is solvable in $\mathrm{O}(N_{tot})$. If E is invertible the system is well posed [35] and the interconnecting variables can be computed in a centralized block before the integration of each subsystem.

The same approach can still be applied if the other strings are added to the picture. The constraints imposed by the connection between strings can be added to E. The augmentation of E may change its structure; but we will show that these constraints can still be managed efficiently.

In the remainder of the section, we will first show that the single subcell can be cast into a string of interconnected systems and subsequently we will address the inter-string constraints.

B. Spatially Interconnected Li-ion Subcell Model

Let us consider the generic subcell of Fig. 6, Fig. 7 shows the k^{th} finite element with the definition of its state and interfacing variables. The state equations for the subsystems

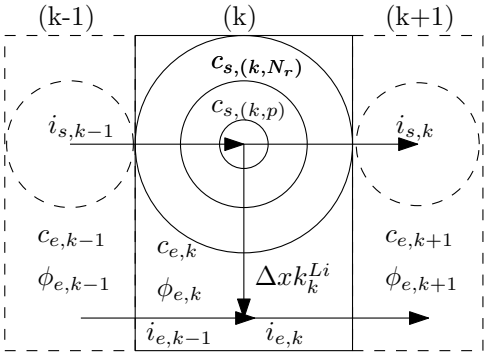

inputs:

$${}^{z}v_k^m = \begin{bmatrix} i_{s,k-1} & \phi_{e,k} & c_{e,k-1} \end{bmatrix}^T$$

$${}^{z}v_k^p = \begin{bmatrix} \phi_{s,k} & i_{e,k} & c_{e,k+1} \end{bmatrix}^T$$

outputs:

$${}^{z}v_{k-1}^m = \begin{bmatrix} \phi_{s,k} & i_{e,k-1} & c_{e,k} \end{bmatrix}^T$$

$${}^{z}v_{k+1}^p = \begin{bmatrix} i_{s,k} & \phi_{e,k+1} & c_{e,k} \end{bmatrix}^T$$

states

$${}^{z}x_k = \begin{bmatrix} c_{s,(k,1)}, \ldots, c_{s,(k,p)}, \ldots, c_{s,(k,N_r)}, c_{e,k} \end{bmatrix}^T$$

Fig. 7. A single discretized part of positive / negative electrode interconnected with neighboring blocks delimited by dashed lines.

are the N_r dynamic equations for the solid and one for the electrolyte diffusion. They depend on j_k^{Li}. By eliminating ϕ_{sk} from equation (1) using the charge balance in the solid phase and then eliminating i_{sk} using the relation between the volumetric rate of electrochemical reaction and the gradient of the current in the solid phase, we get j_k^{Li} as an implicit function of states, inputs but also j_k^{Li} itself. Its linearization yields the explicit form (as also done in [36]):

$$j_k^{Li} = \frac{a_s}{R_{ct}} \left[\phi_{sk} - \phi_{ek} - U\left(c_{s(k,N_r)}\right) \right] \tag{14}$$

where,

$$R_{ct} = \frac{RT}{j_0 F \left(\alpha_a + \alpha_c\right)}$$

Fig. 8 plots the comparison between computing j^{Li} by solving the nonlinear nonlinear Butler-Volmer kinetics and by using (14) for values of the overpotential covering the range obtained in all the simulations discussed in the paper. The analysis shows that the linearization error is of the order of 1% at most. Substituting the linearized j_k^{Li} in the dynamic

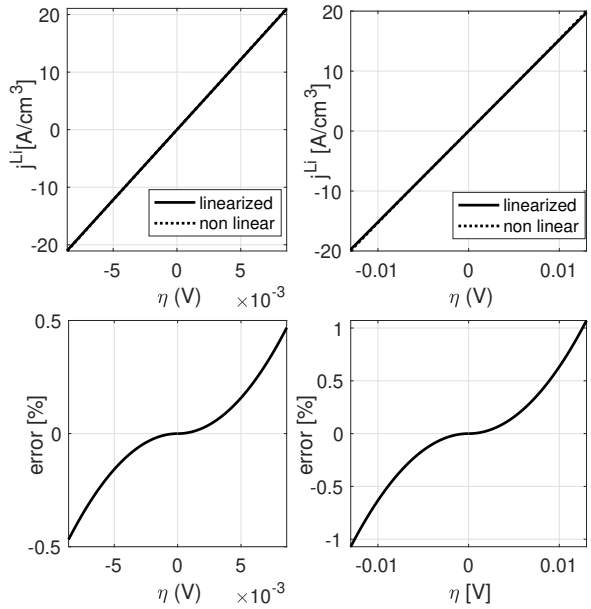

Fig. 8. Results of the transient current simulation: current, voltage and temperature.

equations, we obtain the following state equations, that employ the definitions of the variables given in Fig. 7

$$\dot{x}_k = \begin{bmatrix} -\alpha_1 & \alpha_1 & 0 & \ldots & 0 \\ \frac{D_s}{\Delta r^2} & -\alpha_2 & \alpha_2 & \ldots & 0 \\ \ldots & \ldots & \ldots & \ldots & \ldots \\ 0 & \ldots & \frac{D_s}{\Delta r^2} & -\frac{D_s}{\Delta r^2} & 0 \\ 0 & \ldots & 0 & 0 & -\frac{2D_e^{eff}}{\epsilon_e \Delta x^2} \end{bmatrix} x_k + \begin{bmatrix} 0 \\ 0 \\ \ldots \\ -\Omega\, U\left(x_k\left(N_r\right)\right) \\ -\gamma\, U\left(x_k\left(N_r\right)\right) \end{bmatrix} + \begin{bmatrix} 0 & 0 & 0 \\ 0 & 0 & 0 \\ \ldots & & \ldots \\ \Omega & 0 & 0 \\ \gamma & 0 & \frac{D_e^{eff}}{\epsilon_e \Delta x^2} \end{bmatrix} v_k^p + \begin{bmatrix} 0 & 0 & 0 \\ 0 & 0 & 0 \\ \ldots & & \ldots \\ \Omega \frac{\Delta x}{\sigma^{eff}} & -\Omega & 0 \\ \gamma \frac{\Delta x}{\sigma^{eff}} & -\gamma & \frac{D_e^{eff}}{\epsilon_e \Delta x^2} \end{bmatrix} v_k^m \tag{15}$$

where

$$\Omega = -\frac{1}{\beta R_{ct}} \left(\frac{2}{N_r \Delta r F} + \frac{1}{\Delta r F} \right) \quad \gamma = \frac{a_s}{\beta R_{ct}} \left(\frac{1 - t_+^0}{F} \right)$$
$$\beta = 1 + \frac{\Delta x^2}{\sigma^{eff}} \frac{a_s}{R_{ct}} \quad \alpha_i = \left(\frac{2D_s}{i \Delta r} + \frac{D_s}{\Delta r^2} \right) \tag{16}$$

and, defining some constants

$$\begin{aligned} M_1 = \tfrac{\Delta x a_s}{\beta R_{ct}} \quad M_2 = \tfrac{\Delta x^2}{\sigma^{eff}} \tfrac{a_s}{\beta R_{ct}} \\ M_3 = \tfrac{\Delta x}{\sigma^{eff}} \quad M_4 = -\tfrac{\Delta x}{\kappa^{eff}} \quad K_d K = \tfrac{\kappa_D^{eff}}{\kappa^{eff}}, \end{aligned} \tag{17}$$

the output relation equations can be derived as

$$\begin{aligned} v_{k-1}^p = \begin{bmatrix} M_2 U\left(x_k\left(N_r\right)\right) \\ M_1 U\left(x_k\left(N_r\right)\right) \\ x_k\left(N_r+1\right) \end{bmatrix} + \begin{bmatrix} (1-M_2) & 0 & 0 \\ -M_1 & 1 & 0 \\ 0 & 0 & 0 \end{bmatrix} v_k^p \\ + \begin{bmatrix} M_3\left(1-M_2\right) & M_2 & 0 \\ -M_2 & M_1 & 0 \\ 0 & 0 & 0 \end{bmatrix} v_k^m \end{aligned} \tag{18}$$

$$\begin{aligned} v_{k+1}^m = \begin{bmatrix} M_1 U\left(x_k\left(N_r\right)\right) \\ K_d K \ln\left(x_k\left(N_r+1\right)\right) \\ x_k\left(N_r+1\right) \end{bmatrix} \\ + \begin{bmatrix} -M_1 & 0 & 0 \\ 0 & M_4 & 0 \\ 0 & 0 & 0 \end{bmatrix} v_k^p + \begin{bmatrix} -\left(M_2-1\right) & M_1 & 0 \\ 0 & 1 & 0 \\ 0 & 0 & 0 \end{bmatrix} v_k^m \\ + \begin{bmatrix} 0 \\ -K_d K \ln\left(v_k^p\left(N_r\right)\right) \\ 0 \end{bmatrix}. \end{aligned} \tag{19}$$

The separator and the interfaces between the terminals and the electrodes and the electrodes are amenable to the same procedure. One only needs to take special care to ground the solid potential on any one cell, by imposing $\phi_s = 0$. If this is not done, the interconnected system looses well posedness - see comment on invertibility of E above. This results in a system in the form of (9). From the analysis of the above system, two conclusions are due: (1) the interconnecting output variables are only weakly coupled to the Li diffusion in the active material; in fact only the last element $x_k(N_r)$ appears in the above equations. (2) Although the subsystems are not directly in the *linear in interconnecting variables* form, the only nonlinear term in the equation depends on $v_k^p\left(N_r\right)$ which is a state of the neighboring block and is thus available for solving the system $Ev = b$.

Following the above procedure, one gets to N_c independent set of equations; each string has as inputs the current flowing in that subcell ($\widehat{I}_z$) and the temperature, while its output is the terminal voltage. At this stage the subcell current is still undetermined. Recall now that the N_c cells are connected in parallel, this imposes the constraints (7) and (8). Including these constraints in the above formulation, one gets:

$$\begin{bmatrix} E_{tot} & \mathbf{0}_{N_c \times N_c} \\ C_{v,tot} & C_{I,tot} \\ \mathbf{0}_{1 \times N_c} & \mathbf{1}_{1 \times N_c} \end{bmatrix} \begin{bmatrix} v_{tot} \\ I_{tot} \end{bmatrix} = \begin{bmatrix} b_{tot} \\ \mathbf{0}_{N_c \times 1} \\ I \end{bmatrix} \tag{20}$$

where the unknown v_{tot} and I_{tot} are respectively the stacked vector of the v for each subcell and stacked vector of the subcell currents. Similarly, b_{tot} is the stacked vector of all b. E_{tot} is the block-diagonal matrix of E defined above; $[C_{v,tot}\, C_{I,tot}]$ is the $(N_c - 1) \times 2N_c$ matrix that selects the potential of the first element of the negative and the last element of the positive electrode and the current for pairs of subcell according to (3) to impose the constraint (8). The bottom row of (20) translates (7) in matrix form.

Inspection of (20) reveals that the addition of the parallel constraints breaks the SSS structure; however one notices that the equations are in the form of a block triangular system of equations. This means that at each sampling time, the SSS systems of equation of the form $Ev = b$ can be solved independently as in the case of the single subcell and subsequently, the subcell currents can be computed solving the bottom half of the system.

We thus define the integration routine summarized in Fig. 9: at each integration step, the state dependent parameters are

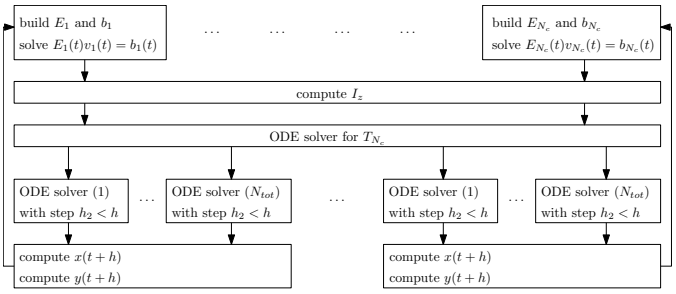

Fig. 9. Graphical representation of the integration routine of the SSS model.

updated according to the previously computed value of the states; these values are entered in the E_z matrices and the b_z vectors. The SSS algebra is used to solve for the interconnected variables v at a sampling step h. The interconnecting variables v along with the other variables compute the current through each subcell. The current through each subcell along with the electrochemical variable available in v drives the discretized thermal dynamics. After that, all the sub-systems of each subcell can be simulated using an ODE solver of choice keeping the interconnecting variables and subcell temperature constant.

V. Model Analysis and Results

This section analyzes the simulation results of the proposed model. We focus on mainly two aspects: comparison with the complete computation fluid dynamics (CFD) model and computational efficiency analysis. The reference cell model is the one in [15], [31].

A. Model Comparison

The proposed integration scheme requires some assumptions and simplifications. In order to assess the effects of these simplifications, we compare the outputs and states of our model against the experimentally validated CFD model presented in [36] and using the same inputs for an easier comparison. The choice of using a CFD model allows for a more accurate comparison of the internal variables which are not easily measurable. The model validation details three main aspects terminal voltage, concentration gradients along x, and response to transient currents. Being based on a finite

difference approach, the discretization resolution affects computation time and accuracy. One has to chose the discretization based on the scope of the model and the computational resources. The choice of the discretization level is a delicate topic as a too coarse discretization can lead to inaccurate results. In this work, we chose the proposed discretization by trying progressively finer discretizations (and time steps) until we observed that the terminal voltage and the solid phase surface concentration converged to the same values. We then used the coarser discretization that yields that convergence, that is $N_n = N_p = 5$, $N_s = 3$, $N_r = 50$, $N_c = 6$ and $h = 0.05s$. The next subsection investigates the impact of the discretization on the computational efficiency.

Fig. 10 plots the results of a constant current discharge experiment performed from a fully charged battery with three current levels. We consider two types of simulations, the first one (solid line) neglects the temperature dynamics (considering all subcells at the same temperature). The second type of simulation considers the entire model as described. The plot

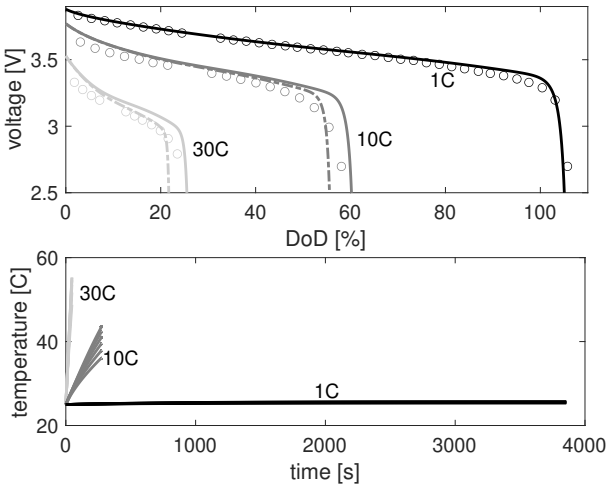

Fig. 10. Terminal voltage prediction at different C-rates: discretized model neglecting the temperature dynamics (solid line), discretized model considering temperature dynamics (dashed line), and CFD model (o).

shows the terminal voltage in the top plot and the temperature dynamics for each of the N_c subcells, in the bottom. The terminal voltage is plotted with respect to the depth of discharge (DoD), whereas the temperature is time-based. From figure, a numbers of conclusions are due:

- the model is accurate in the entire DoD range for 1C; for higher currents the accuracy range is reduced toward the end of discharge. The error at higher currents is due to the nonlinearity in the terminal voltage characteristic $U(c_{s,e})$. Because of that, small errors in $c_{s,e}$ result in large errors in voltage.
- In the case of 1 C, the temperature dynamics do not play an important role. 1 C is not enough to heat the battery. As the C rate increases, we see that the temperature dynamics considerably affect the discharge dynamics.
- For the higher C rates, as shown in the bottom plot of the figure, a temperature gradient builds in the cell. At the end of the discharge the temperature difference between the core and the surface of the cell gets to 20 degrees.

One of the advantages of using an electrochemical model resides in the possibility of accurately modeling the evolution of the species gradients. Fig. 11 compares the proposed model and the CFD model. The figure provides a snapshot during a constant current (5 C) discharge of the electrochemical reaction at the solid/ electrolyte interface j^{Li}, the surface concentration and the Li concentration in the electrolyte as a function of the position. The model correctly describes the

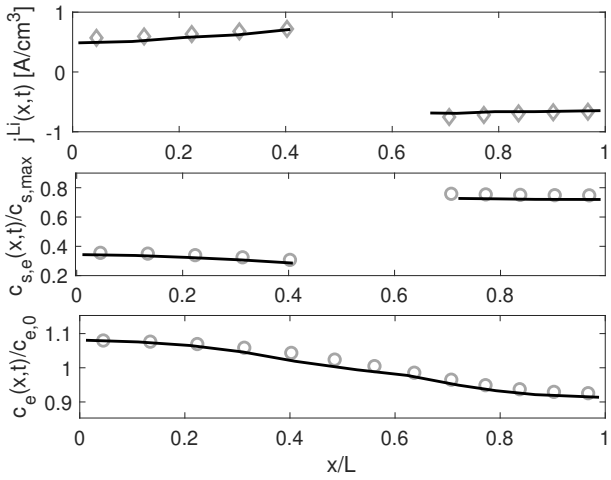

Fig. 11. Gradients along the x dimension. The continuous line is the CFD model, whereas the circles represent our discretized model.

gradients along the x direction.

Fig. 12 plots the terminal voltage and the temperature evolution for a series of current steps. Also in this case,

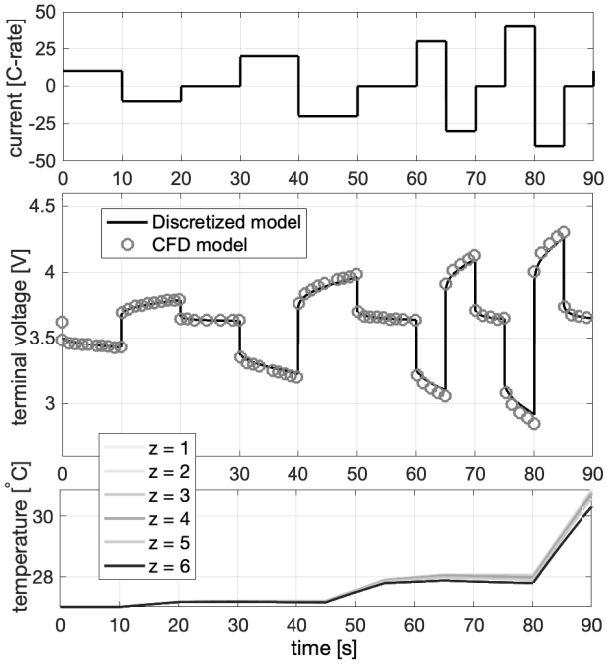

Fig. 12. Results of the transient current simulation: current, voltage and temperature. In the last plot, z indicates the index of the thermal subsystems.

This article has been accepted for publication in a future issue of this journal, but has not been fully edited. Content may change prior to final publication. Citation information: DOI 10.1109/TIE.2020.3008377, IEEE Transactions on Industrial Electronics

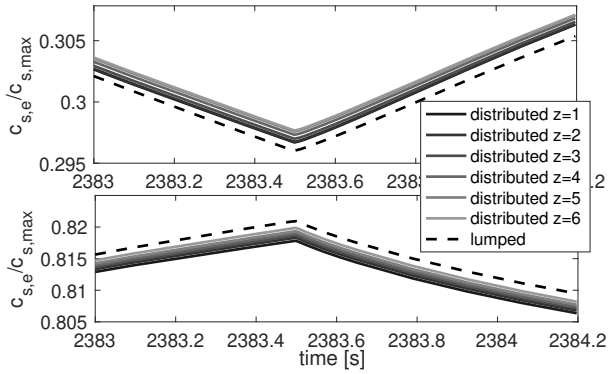

Fig. 13. Comparison of the concentrations dynamics. z indicates the index of the thermal subsystems.

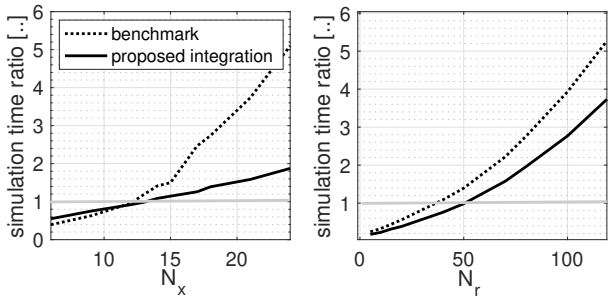

Fig. 14. Simulation time per step for different discretization levels.

the model correctly captures the voltage dynamics. Note that despite the extremely high currents, this short test does not develop an appreciable temperature gradient.

Fig. 13 illustrates the advantages of a coupled bi-directional and spatially distributed thermal model. It plots the comparison of the surface concentration dynamics in the first element of the negative electrode (top subplot) and in the last element of the positive electrode (bottom subplot) for the lumped thermal model ($N_c = 1$ - dashed line) and for the distributed model ($N_c = 6$ - solid line); the darkest solid line refers to the inner subcell, while the lighter solid line refers to the outer subcell. The simulation considers a dynamic current request characterized by alternating charging and discharging events - this is reminiscent of what happens in hybrid electric vehicles or, to a lesser extend, solar power battery packs.

The temperature affects the intercalation dynamics, therefore, if the internal temperature gradient is not negligible, the lithium concentration is not uniform along the radial direction r^c.

B. Complexity Analysis

The use of the spatially interconnected framework enables two computational advantages: 1) the coupling equations can be solved in linear complexity with respect to the discretization along x, and 2) the integration is amenable to a high degree of parallelization. In fact, recalling Fig. 9, the integration of each cell can be run in parallel. Fig. 14 shows the simulation time ratio for different discretization levels of positive electrode, negative electrode and separator keeping the discretization of spherical active material particle constant and the computation time for varying radial discretizations. The simulation time ratio is the ratio between the time it takes to simulate a given time interval and the duration of that time interval. The figure compares this index for an implementation of the model that does not exploit the spatially interconnected framework and the proposed approach. It is worth noting that the baseline against which our approach is compared represents the computational complexity of the traditional P2D model augmented with the distributed thermal model. From figure, one can note that

- increasing the discretization along x causes a linear increase in the simulation time. Whereas, in the traditional approach, the increase in computation time is more than linear.
- For low levels of discretization, the proposed method comes with an overhead that makes the traditional approach more efficient. As a matter of fact, the largest gain in terms of simulation time are reached for N_x above the real time limit of the current hardware. Nevertheless, one should focus on the order of the complexity.
- When the radial discretization increases, the simulation time does not grow linearly as the method does not exploit any structure in the r dimension.
- Considering the current computer, the proposed framework allows the user to increase the real time limit from $N_x = 10$ to $N_x = 14$, if N_r is kept constant or from $N_r = 40$ to $N_r = 50$, if N_x is kept constant. The increase on N_r is particularly appreciated because it considerably improves the accuracy of the solid phase diffusion phenomena of Li ions.

The above analysis indicates that the chosen discretization of $N_r = 50$, $N_n = 5$, $N_p = 5$, $N_s = 3$, and $N_c = 6$ is at the limit of real time implementation.

VI. Conclusions

This work presents a coupled thermal-electrochemical coupled, control-oriented electrochemical model of a Li-ion cell that accounts for the thermal dynamics. The use of the finite difference discretization scheme yields a spatially interconnected system. Exploiting minor approximations, the complexity of integrating the equation can be considerably reduced. The proposed modeling approach, relying only on two approximations (linearization of the Butler-Volmer Kinetics and the holding of the interconnecting variables), has several advantages:

- It provides an efficient simulator that captures the mass diffusion dynamics of the Li-ion cell and the thermal gradients of the cell battery;
- it avoids any iterative solution of nonlinear equations, thus improving efficiency and avoiding possible non convergent behavior;
- when linearized, the state space model assumes an SSS structure that can further exploited in the design and implementation of control systems as shown in [26], [29], [30] and thus makes it a control-oriented model;
- it is amenable to parallelization, thus improving even further its computational efficiency.

REFERENCES

[1] Satadru Dey, Hector E Perez, and Scott J Moura. Model-based battery thermal fault diagnostics: Algorithms, analysis, and experiments. *IEEE Transactions on Control Systems Technology*, 27(2):576–587, 2017.

[2] P.W.C. Northrop, B. Suthar, V. Ramadesigan, S. Santhanagopalan, R. D. Braatz, and V.R. Subramanian. Efficient simulation and reformulation of lithium-ion battery models for enabling electric transportation. *Journal of The Electrochemical Society*, 161(8):E3149–E3157, 2014.

[3] K. Li, F. Wei, K. J. Tseng, and B. Soong. A practical lithium-ion battery model for state of energy and voltage responses prediction incorporating temperature and ageing effects. *IEEE Transactions on Industrial Electronics*, 65(8):6696–6708, Aug 2018.

[4] S Allu, S Kalnaus, S Simunovic, J Nanda, JA Turner, and S Pannala. A three-dimensional meso-macroscopic model for li-ion intercalation batteries. *Journal of Power Sources*, 325:42–50, 2016.

[5] M. Doyle, T. Fuller, and J Newman. Modeling of galvanostatic charge and discharge of the lithium/polymer/insertion cell. *Journal of the Electrochemical Society*, 140(6):1526–1533, 1993.

[6] T. F Fuller, M. Doyle, and J. Newman. Simulation and optimization of the dual lithium ion insertion cell. *Journal of the Electrochemical Society*, 141(1):1–10, 1994.

[7] K. Smith and C-Y. Wang. Solid-state diffusion limitations on pulse operation of a lithium ion cell for hybrid electric vehicles. *Journal of Power Sources*, 161(1):628–639, 2006.

[8] N. A. Chaturvedi, R. Klein, J. Christensen, J. Ahmed, and A. Kojic. Algorithms for advanced battery-management systems. *IEEE Control Systems*, 30(3):49–68, 2010.

[9] A.M. Bizeray, S. Zhao, S. Duncan, and D. A. Howey. Lithium-ion battery thermal-electrochemical model-based state estimation using orthogonal collocation and a modified extended kalman filter. *CoRR*, abs/1506.08689, 2015.

[10] Y. Zeng, P. Albertus, R. Klein, N. Chaturvedi, A. Kojic, M. Z Bazant, and J. Christensen. Efficient conservative numerical schemes for 1D nonlinear spherical diffusion equations with applications in battery modeling. *Journal of The Electrochemical Society*, 160(9):A1565–A1571, 2013.

[11] D. Zhang, B. N Popov, and R. E. White. Modeling lithium intercalation of a single spinel particle under potentiodynamic control. *Journal of The Electrochemical Society*, 147(3):831–838, 2000.

[12] A. Jokar, B. Rajabloo, M. Désilets, and M. Lacroix. Review of simplified pseudo-two-dimensional models of lithium-ion batteries. *Journal of Power Sources*, 327:44–55, 2016.

[13] G. G Botte, V. R. Subramanian, and R.E White. Mathematical modeling of secondary lithium batteries. *Electrochimica Acta*, 45(15):2595–2609, 2000.

[14] C. Forgez, Dinh V. Do, G. Friedrich, M. Morcrette, and C. Delacourt. Thermal modeling of a cylindrical lifepo 4/graphite lithium-ion battery. *Journal of Power Sources*, 195(9):2961–2968, 2010.

[15] Y. Kim, J.B. Siegel, and A.G Stefanopoulou. A computationally efficient thermal model of cylindrical battery cells for the estimation of radially distributed temperatures. In *American Control Conference (ACC), 2013*, pages 698–703. IEEE, 2013.

[16] Eric Prada, D Di Domenico, Yann Creff, J Bernard, Valérie Sauvant-Moynot, and François Huet. Simplified electrochemical and thermal model of lifepo4-graphite li-ion batteries for fast charge applications. *Journal of The Electrochemical Society*, 159(9):A1508–A1519, 2012.

[17] Dong Zhang, Satadru Dey, Hector E Perez, and Scott J Moura. Real-time capacity estimation of lithium-ion batteries utilizing thermal dynamics. *IEEE Transactions on Control Systems Technology*, 2019.

[18] Jiuchun Jiang, Haijun Ruan, Bingxiang Sun, Weige Zhang, Wenzhong Gao, Linjing Zhang, et al. A reduced low-temperature electro-thermal coupled model for lithium-ion batteries. *Applied Energy*, 177:804–816, 2016.

[19] Xinfan Lin, Hector E Perez, Shankar Mohan, Jason B Siegel, Anna G Stefanopoulou, Yi Ding, and Matthew P Castanier. A lumped-parameter electro-thermal model for cylindrical batteries. *Journal of Power Sources*, 257:1–11, 2014.

[20] S Panchal, I Dincer, M Agelin-Chaab, R Fraser, and M Fowler. Thermal modeling and validation of temperature distributions in a prismatic

[21] Sun Ung Kim, Paul Albertus, David Cook, Charles W Monroe, and Jake Christensen. Thermoelectrochemical simulations of performance and abuse in 50-ah automotive cells. *Journal of Power Sources*, 268:625–633, 2014.

lithium-ion battery at different discharge rates and varying boundary conditions. *Applied Thermal Engineering*, 96:190–199, 2016.

[22] Adrien M Bizeray, Shi Zhao, Stephen R Duncan, and David A Howey. Lithium-ion battery thermal-electrochemical model-based state estimation using orthogonal collocation and a modified extended kalman filter. *Journal of Power Sources*, 296:400–412, 2015.

[23] Billy Wu, Vladimir Yufit, Monica Marinescu, Gregory J Offer, Ricardo F Martinez-Botas, and Nigel P Brandon. Coupled thermal–electrochemical modelling of uneven heat generation in lithium-ion battery packs. *Journal of Power Sources*, 243:544–554, 2013.

[24] K. Somasundaram, E. Birgersson, and A. S. Mujumdar. Thermal–electrochemical model for passive thermal management of a spiral-wound lithium-ion battery. *Journal of Power Sources*, 203:84–96, 2012.

[25] M. Corno, N. Bhatt, and M. Verhaegen. An efficient control oriented modeling approach for lithium ion cells. In *American Control Conference (ACC), 2012*, pages 4733–4738. IEEE, 2012.

[26] J. K. Rice and M.Verhaegen. Distributed control: A sequentially semi-separable approach for spatially heterogeneous linear systems. *IEEE Transactions on Automatic Control*, 54(6):1270 – 1283, Jun 2009.

[27] Scott J Moura, Federico Bribiesca Argomedo, Reinhardt Klein, Anahita Mirtabatabaei, and Miroslav Krstic. Battery state estimation for a single particle model with electrolyte dynamics. *IEEE Transactions on Control Systems Technology*, 25(2):453–468, 2016.

[28] Ngoc Tham Tran, Mahinda Vilathgamuwa, Troy Farrell, San Shing Choi, Yang Li, and Joseph Teague. A padé approximate model of lithium ion batteries. *Journal of The Electrochemical Society*, 165(7):A1409–A1421, 2018.

[29] Edwin van Solingen, Jan-Willem van Wingerden, Patricio Torres, Justin Rice, Roeland de Breuker, and Michel Verhaegen. Parameter estimation for spatially interconnected descriptor systems using sequentially semi-separable matrices. In *American Control Conference (ACC), 2013*, pages 1657–1662. IEEE, 2013.

[30] Justin K Rice and Michel Verhaegen. Efficient system identification of heterogeneous distributed systems via a structure exploiting extended kalman filter. *IEEE Transactions on Automatic Control*, 56(7):1713–1718, 2011.

[31] K. Smith and C-Y. Wang. Power and thermal characterization of a lithium-ion battery pack for hybrid-electric vehicles. *Journal of power sources*, 160(1):662–673, 2006.

[32] WB Gu and CY Wang. Thermal-electrochemical modeling of battery systems. *Journal of The Electrochemical Society*, 147(8):2910–2922, 2000.

[33] S. Anwar, C. Zou, and C. Manzie. Distributed thermal-electrochemical modeling of a lithium-ion battery to study the effect of high charging rates. *IFAC Proceedings Volumes*, 47(3):6258–6263, 2014.

[34] Uri M Ascher. *Numerical methods for evolutionary differential equations*, volume 5. Siam, 2008.

[35] R. D'Andrea and G. E. Dullerud. Distributed control design for spatially interconnected systems. *IEEE Transactions on Automatic Control*, 48(9):1478 – 1495, sept 2003.

[36] K. Smith, C. D. Rahn, and C-Y. Wang. Control oriented 1d electrochemical model of lithium ion battery. *Energy Conversion and management*, 48(9):2565–2578, 2007.

Matteo Corno received the Master of Science degree in computer and electrical engineering from the University of Illinois, and the Ph.D. cum laude degree with a thesis on active stability control of two-wheeled vehicles from the Politecnico di Milano, Milano, Italy, in 2005 and 2009. He is an Associate Professor with the Dipartimento di Elettronica, Informazione e Bioingegneria, Politecnico di Milano, Italy. His current research interests include dynamics and control of vehicles (especially electric-hybrid vehicles), Lithium-ion battery modeling, estimation and control. He held research positions at Thales Alenia Space, Harley Davidson, U. of Minnesota, Johannes Kepler University in Linz, and TU Delft.